The Messinian 'Vena del Gesso' evaporites revisited: characterization of isotopic composition and organic matter

S. LUGLI[1], M. A. BASSETTI[2 *], V. MANZI[3], M. BARBIERI[4], A. LONGINELLI[3] & M. ROVERI[3]

[1]*Dipartimento di Scienze della Terra, Università degli Studi di Modena e Reggio Emilia, Largo S. Eufemia 19, 41100 Modena, Italy (e-mail: lugli.stefano@unimore.it)*

[2]*IUEM0-UMR, 6538 Place Copernic, 29280 Plouzanè, France*

[3]*Dipartimento di Scienze Geologiche, Università di Parma, Parco Area delle Scienze 157/A, 43100, Parma, Italy*

[4]*Dipartimento di Scienze della Terra, Università 'La Sapienza', Piazzale Aldo Moro, 00185 Roma, Italy*

**Present Address: LEGEM, Université de Perpignan, 52 Avenue Paul Alduy, 66860 Perpignan, France*

Abstract: The 'Vena del Gesso' (Gessoso-Solfifera Fm, Messinian) is a 227 m-thick ridge along the western Romagna Apennines (Italy) consisting of up to 16 selenite cycles separated by shales and minor carbonate. The total organic carbon values of these deposits range between 0.087–0.016% (gypsum) and 3% (shales). Organic matter is dominated by black debris associated with continental debris. Algae and dynocysts are rare (<1%). The amount of amorphous organic matter is low but it may reach up to *c.* 40%. The $^{87}Sr/^{86}Sr$ of gypsum and carbonate vary from 0.708890 to 0.709024, yielding non-oceanic values with several exceptions that plot within error of coeval oceanic values only in the upper part of the section (from the 6° bed). The sulphur isotope composition of gypsum range between $\delta^{34}S = +21.8$ and $+23.7‰$ and may represent precipitation of $\delta^{34}S$-enriched gypsum due to the fractionation effect or recycling of coeval gypsum with contributions of brine-sediment redox variations. The isotope values of carbonates show a large variability ($-6.4 < \delta^{18}O < +6.05‰$; $-14.68 < \delta^{13}C < +2.5‰$), suggesting a complex origin by mixing of marine and non-marine waters with a significant contribution of reduced organic matter. These data point to an evaporite basin dominated by continental waters which received significant phases of marine recharge in the upper part together with a marked facies change. Because seawater recharges and a similar facies change are present in other Messinian sections, it follows that we have new possible geochemical and facies markers to correlate the Lower Evaporites across the Mediterranean.

Isotope stratigraphy represents a fundamental tool in palaeoenvironmental and palaeoclimate reconstruction, especially for evaporite sediments. The integration of geochemical data is imperative in facies interpretation, as the peculiar and restricted setting of evaporite deposition makes the use of geochemical data problematic. This is because brine composition may be the result of a mixture of marine and continental water, and sediment composition may be strongly influenced by recycling of older sediments, biologic activity and diagenesis. These uncertainties may be overcome only with the integration of geochemical data in a detailed stratigraphic and facies framework.

This integration is particularly needed for the Messinian evaporites in the Mediterranean, because their origin is still debated and because many of the available isotope data are scattered and commonly obtained from sections whose stratigraphy is not well constrained in the regional framework. The information provided by such scattered data is very difficult to interpret if its significance is not correctly placed into the salinity crisis framework. This is probably one of the reasons why the debate still exists and even is growing.

This paper illustrates the geochemistry of the Vena del Gesso evaporites (Northern Apennines), which represent the most significant example of detailed facies stratigraphy for the Lower Evaporites in the Mediterranean. The aim is to discuss new possible stratigraphic markers to correlate the elusive evaporite sediments across the Mediterranean during the Messinian salinity crisis.

From: SCHREIBER, B. C., LUGLI, S. & BĄBEL, M. (eds) *Evaporites Through Space and Time.* Geological Society, London, Special Publications, **285**, 179–190.
DOI: 10.1144/SP285.11 0305-8719/07/$15.00

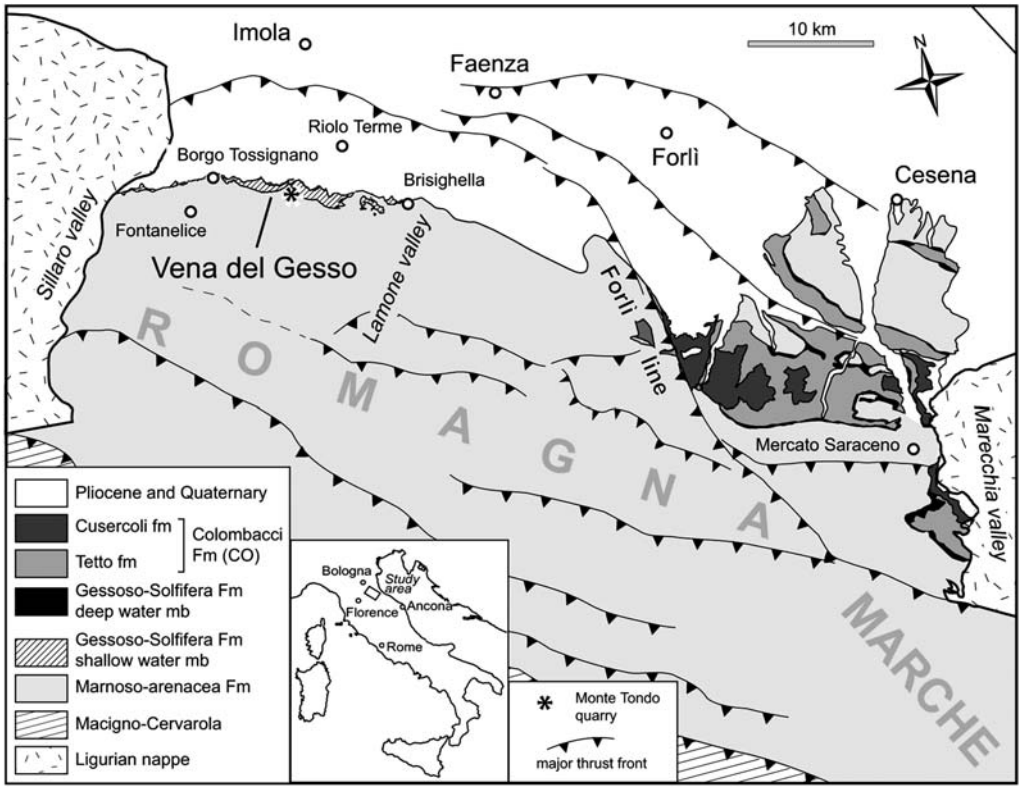

Fig. 1. Schematic geological map of the Romagna Apennines.

Geological setting and stratigraphy

The Romagna Apennines extends from the Sillaro valley to the west and to the Marecchia valley to the east (Fig. 1). This portion of the chain can be subdivided into two minor basement-detached units affected by fold-and-thrust structures (Barchi *et al.* 1998): (1) a lower and older one composed of Mesozoic to Cenozoic carbonates; and (2) an upper one, up to 3500 m-thick, consisting of a lower Miocene–Quaternary siliciclastic wedge representing the deep-water to continental infill of successive foredeep basins progressively migrating toward the NE, ahead of the advancing Apennines thrust belt (Ricci Lucchi 1986).

According to Roveri *et al.* 2003, the upper unit of the Romagna Apennines can be subdivided into four formations ranging from Langhian to Pliocene (Vai 1988):

(1) The Marnoso-arenacea Formation (Langhian–Messinian) mainly consists of deep-water siliciclastic turbidites representing the sedimentary infill of the Adriatic foredeep. In the upper part a clayey unit, mainly consisting of slope mudstones ('ghioli di letto') contains minor turbiditic sandstones and chaotic bodies; these deposits are capped by a thin horizon of cyclically interbedded organic-rich laminites and mudstones, informally named 'euxinic shales' (upper Tortonian–lower Messinian). The well-defined biomagnetostratigraphic events recognized within this unit (Vai 1997; Krijsman *et al.* 1999) allow a detailed correlation with other pre-evaporitic successions of the Mediterranean (Tripoli Formation of Sicily and Spain). The euxinic shales unit, recording the palaeoceanographic changes that affected the whole Mediterranean area before the Messinian Salinity Crisis, contains the Tortonian–Messinian boundary and spans a 1.5 million year time interval.

(2) The Gessoso-solfifera Formation (Messinian) is made up of both primary (Vena del Gesso, Vai & Ricci Lucchi 1977; Table 1) and clastic, resedimented evaporites with interbedded organic-rich shales (eastern Romagna and Marche area), deposited during the evaporitic and post-evaporitic

Table 1. *Facies description of the Vena del Gesso evaporites (from Vai & Ricci Lucchi 1977)*

Facies	Description
F1 Bituminous shale	Organic-rich, laminated marly clay, containing abundant vegetal, fish and insect remains
F2 Calc-gypsum stromatolite and selenite, calcareous breccia and sandstone, flat-lying selenite	Laminated calc-gypsum limestone of algal origin, selenite enclosing algal laminae, mechanically reworked stromatolite clasts, fine-to very coarse sandstone composed of gypsum and carbonate grains, loose selenite crystals lying on their long axis
F3 Massive selenite	Vertical selenite crystals enclosing algal filaments
F4 Banded selenite	Alternation of autochthonus and clastic selenite, with muddy carbonates draping dissolution surfaces
F5 Nodular, lenticular and flaser-bedded gypsum	Clastic selenite with lenses of siltstone, sandstones and micritic carbonate, presence of diagenetic structures
F6 Chaotic gypsum	Mixture of selenite crystal of variable sizes in clayey matrix, clay chips, wood fragments

stages of the Messinian Salinity Crisis (Manzi *et al.* 2005).

(3) The Colombacci Formation (upper Messinian), consisting of siliciclastic sediments derived from Apenninic sources, was variably deposited in both shallow and deep brackish or freshwater basins developed during the final phase of the Messinian Salinity Crisis (Lago–Mare stage; Bassetti *et al.* 2004).

(4) The Argille Azzurre Formation (lower Pliocene) is made up of deep marine mudstones recording the return to fully marine conditions.

According to most recent physical stratigraphic frameworks (Roveri *et al.* 1998, 2001, 2003, 2004, Manzi *et al.* 2005), the deposition of the Messinian evaporites within the upper unit was controlled by a tectonically related basin topography which began to develop in the upper Tortonian. Primary evaporites (Vena del Gesso) were precipitated in thrust-top semi-closed basins, whereas in the deeper portion of the foredeep only dark euxinic shales were deposited. Additionally, during the post-evaporitic phase clastic evaporites, a large variety of gravity-driven deposits deriving from the dismantlement of the Vena del Gesso primary evaporites, were also deposited in the deep basins.

The 'Vena del Gesso' is a NW–SE elongated relief, approximately 15 km in length, located in the northern Apennines between the Sillaro and the Lamone river valleys. This feature consists of a 227 m-thick succession of 16 cycles of Messinian evaporites. Their deposition was controlled by astronomical precession in a time span ranging from 5.96 to 5.61 $\pm$ 0.02 Ma (Krijsmann *et al.* 1999). The Vena del Gesso evaporites were earlier taken as an example for the formulation of the sedimentary model for the cyclical deposition of primary selenitic gypsum (Vai & Ricci Lucchi 1977, Marabini & Vai 1985). We are currently revising the facies interpretation (Lugli *et al.* 2005), but in this paper we refer to the original facies description of Vai & Ricci Lucchi (1977; Table 1).

Materials and methods

Detailed sedimentological observations were carried out in the Monte Tondo quarry section and the entire evaporite succession was measured and sampled. A total of 100 samples of gypsum, carbonates and shales have been collected and some of these samples were selected for petrographic and geochemical investigations. The scope of the selection was to provide at least one sample for each facies in the stratigraphic column, following the facies classification proposed by Vai & Ricci Lucchi (1977; Table 1). Because the cycles are thicker and with fewer variations in facies (F3 and F4) in the lower part of the section, samples are more numerous in the upper part, where cycles are thinner but show the complete facies association (F3–F6). For these reasons, the apparent higher frequency of samples in the upper part does not represent a sampling bias.

A total of 54 samples were chosen for strontium isotopic analyses. For gypsum analysis, 100 mg of sample were mixed with 1 g of Na_2CO_3 (strontium-free) and treated with 40 ml of bidistilled water for 6 h at 70 °C to obtain pure $Ca(Sr)CO_3$, which was then dissolved with 2.7 M—HCl. After evaporation to dryness, the resulting $Ca(Sr)Cl_2$ was dissolved in HCl and the solution passed through a cation exchange resin to separate strontium. The strontium was then eluted and analysed for $^{87}Sr/^{86}Sr$ ratios by means of a VG Isomass 54E mass spectrometer. The carbonate samples were dissolved with 0.2 M—HCl, and Sr was separated by cation

exchange resin, as previously described for the gypsum samples. For the NBS 987 $SrCO_3$ standard, repeated analyses yielded a mean value of 0.71024 ± 0.00002 (2σ).

The same samples were used to analyse the sulphur isotopic composition: 0.3 g of sulphate by powder was dissolved in distilled water and converted to barium sulphate by adding 0.2 M $BaCl_2$ (~5%) in boiling acid water. The SO_2 gas produced by the sulphates was analysed on a Delta C Finnigan Mat mass spectrometer and all data are expressed in the usual notation as $\delta^{34}S$ ‰ CDT. The standard deviation for $\delta^{34}S$ is ±0.2‰.

Twenty-three bulk carbonate samples were measured for their carbon and oxygen isotopic composition. Measurements were carried out on CO_2 obtained by reaction of $CaCO_3$ with 100% H_3PO_4 at 25 °C and further cryogenic purification in a high vacuum line. The CO_2 isotopic values were measured in a Finnigan Delta S mass-spectrometer vs a CO_2 working standard obtained from a very pure Carrara marble and calibrated periodically vs NBS-19 and NBS-20 international standards. Because our working standard was systematically calibrated over about 45 years against these two NBS standards which, in turn, were calibrated directly vs PDB-1, we report our isotopic results vs the latter reference standard. The results are reported in the usual δ notation. The standard deviation (2σ) of our measurements is ±0.1‰ for oxygen and ±0.08‰ for carbon.

Total organic carbon (TOC) was determined on 51 samples of both shale and gypsum. A total of 40 samples of both gypsum and shale were also treated with HCl and HF, in order to isolate the residual organic matter for a qualitative visual inspection under the optical microscope (palynofacies analysis).

Results

Organic matter

The TOC values ranged between 0.087 and 0.016% in the selenitic facies, but increased up to 3% in the shales separating the gypsum beds (Table 2).

The accumulation of organic carbon and its preservation in evaporitic basins is favoured by the establishment of marked water stratification together with anoxic bottom conditions: the dense brines from which the evaporites are precipitated inhibit the exchange with the overlaying waters and the organic carbon accumulates at a rapid rate. However, the preservation of accumulated organic matter (principally of algal origin in this restricted basin) depends on the consumption of organic carbon by anaerobic bacteria under anoxic/suboxic conditions: many marine microbes require cations to maintain their osmotic balance and the halophilic marine bacteria communities increase their maximum number activity when the salinity reaches 40‰ (Klinkhammer & Lambert 1989).

The amount of organic matter preserved in the samples appears to be quite low. Despite the fact that we cannot estimate accurately the effect of diagenesis on organic matter preservation in these sediments, the geochemical data (see the next section) strongly suggest that bacterial activity was significant during evaporite deposition.

The composition of organic matter (OM) does not vary greatly throughout the section and is typified by the dominance of black debris (oxidized organic matter) that can reach 90% of the identified material. The content of black debris generally increases upsection with the exception of the 8°, 9° and 13° beds. These elements are associated with other types of continental debris such as well-preserved woody fragments, degraded woody debris (not identifiable) leaf cuticles, spores and pollen. As a whole, the proportion of OM of continental origin can reach up to 99% of the total (Table 2, Fig. 2).

Algae and dynocysts are present in very low amounts (<1%) and are very rare. The amount of amorphous organic matter (AOM) that is generally related to a marine origin is low except for a few samples where it reaches up to 39.5% (shale). The AOM is occasionally well-preserved in the gypsum crystals (37.5%) as well. The total amount of AOM shows a marked increase starting from the 7° bed and the highest contents are found in the 8° and 9° beds, where the black debris reaches its lowest concentration (Table 2, Fig. 2).

These palynofacies data show the predominance of continental organic elements during the sedimentation of the Lower Evaporites of the Vena del Gesso basin with low and localized input of marine elements.

Sr ratio

The strontium isotope ratios ($^{87}Sr/^{86}Sr$) of the Vena del Gesso gypsum and carbonate vary from 0.708890 to 0.709024 (Table 2) and are in the range of the Messinian Lower Evaporites in the Mediterranean (Müller & Mueller 1991; Flecker & Ellam 1999; Keogh & Butler 1999; Matano *et al.* 2003; Aharon *et al.* 1993 measured three samples from the base of the 3° bed of of Vena del Gesso, yielding 0.708904–0.708928). Most of the samples yield non-oceanic Sr isotope ratios with several exceptions that plot within error of coeval oceanic waters (McArthur *et al.* 2001; Fig. 3).

According to Flecker & Ellam (2006), Sr isotope ratios diverging from coeval oceanic water values

indicate that the proportion of oceanic water entering the basin was less than *c*. 50% and that brines derived mostly from river run-off and rain waters. Values typical of the coeval global ocean thus represent pulses of direct ingression of oceanic water into a restricted marginal basin characterized by brines deriving from continental waters mixed with less than 50% of oceanic water. These pulses of direct oceanic water ingressions appear only in the upper part of the section, starting from the 6° bed, which is the first showing the complete classic facies assemblage (Vai & Ricci Lucchi 1977), and in particular in the 8° and 9° beds (Fig. 3). The oceanic values measured in the upper part of the section appear in every facies of both gypsum and carbonate, with the exception of massive selenite at the base of each cycle, which is characterized by the lowest recorded values (Table 2). This is probably because massive selenite represents the first depositional product on top of the shales that separate each gypsum cycle. The shales contain large amounts of organic matter, mostly from non-marine sources (see previous section), and thus indicate that the basin was flooded by continental waters just before new evaporitic conditions were established with the precipitation of the massive selenite.

Sulphur isotopes of gypsum

The sulphur isotope compositions of gypsum range between $\delta^{34}S = +21.8$ and $+23.7‰$ (Table 2, Fig. 3). These values are in the range of those measured in the Messinian evaporites of the Mediterranean (Ricchivto & McKenzie 1978; Longinelli 1979; Pierre & Rouchy 1990; Lu & Meyers 2003) and are enriched by about 1–3‰ over the expected value assuming the sulphur isotopic composition of dissolved marine sulphate during the Messinian equal or very close to that of modern oceans.

These values may be interpreted in two different ways. If we accept the conclusions by Thode & Monster (1965), confirmed by Raab & Spiro (1991) concerning the fractionation effect which may take place between dissolved sulphate and solid sulphate during the precipitation of gypsum (enrichment of the solid phase by about 2‰), the measured values may be the result of a primary deposition of sulphate. This implies, obviously, that the sulphur isotopic composition of dissolved marine sulphate during Messinian was equal or very close to that of modern oceanic sulphate (about +21‰ vs CDT, according to the most reliable measurements, Rees (1978), Rees *et al.* (1978). According to the evolution curve through time of the $\delta^{34}S$ of oceanic sulphate (Holser 1977), this hypothesis appears reasonable. However, Pierre & Fontes (1978) suggested a reasonable alternative model to explain the ^{34}S-enriched values. During gypsum precipitation, bacterial activity may easily take place below the brine–sediment interface with sulphate reduction followed by sulfide diffusion through the overlying brine and its partial or total re-oxidation at the brine surface layer in a well oxygenated (^{18}O-enriched) environment (evaporated water and dissolved molecular oxygen). A similar hypothesis has been suggested more recently by Lu & Mayers (2003). Both these hypotheses seem to be theoretically acceptable, independent of gypsum age, as similar enriched $\delta^{34}S$ values were measured in modern Mediterranean salinas (Longinelli 1979; Pierre 1982).

According to Cendón *et al.* (2004) the high $\delta^{34}S$ values (as high as $\delta^{34}S = +23.3‰$) may be the result of recycling of coeval sulphates deposited on the marginal settings. Lower values are generally related to freshwater input or to recycling of ancient evaporites. In Tuscany the recycling of Triassic sulphates ($\delta^{34}S = 14.6‰$) has significantly lowered the $\delta^{34}S$ values of some of the Messinian sulphates ($\delta^{34}S$ ranges from 17.4 to 25.1‰; Dinelli *et al.* 1999). In the northern Apennines we have no evidence of contributions from recycling of older evaporite deposits, first because the Permian evaporites in the Alps and Upper Triassic evaporites in the Apennines were probably not exposed during the Messinian, second because the resulting $\delta^{34}S$ values should be significantly lower than the measured ones.

The highest $\delta^{34}S$ values are grouped in the 8° and 9° beds and then, going upsection, the oscillating curve shows a decrease upward, a trend which is very similar to that of the Sr ratio curve. Exceptions to this trend are noted the uppermost two beds (15° and 16°), where the curve shows the same general trend as noted in the Sr ratio curve but with higher values and larger amplitude for the $\delta^{34}S$ (Fig. 3).

Oxygen and carbon isotopes of carbonate

The isotope values of carbonates show a large variability ($-6.4 < \delta^{18}O < +6.05‰$; $-14.68 < \delta^{13}C < +2.5‰$; Table 2, Fig. 3) and are in the range of other Messinian carbonates associated with evaporites in the Mediterranean (Longinelli 1979; Rouchy & Pierre 1990; Lu *et al.* 2001; Aharon *et al.* 1993 measured two samples from the base of the 3° bed of Vena del Gesso, yielding $-6.09 < \delta^{18}O < -5{,}19‰$ and $-12.43 < \delta^{13}C < -7.85‰$).

Oxygen values range from those characteristic of evaporating brines ($\delta^{18}O$ from +3.34 to +6.05‰) to those characteristic of freshwater ($\delta^{18}O$ from −1.68 to −6.4), whereas negative

Table 2. *Lithology and isotope data of the Vena del Gesso evaporites*

Sample	Distance from base (m)	Bed	Lithology	Facies	$^{87}Sr/^{86}Sr$ gypsum	$^{87}Sr/^{86}Sr$ carbonate	$\delta^{34}S$ (‰ CDT)	$\delta^{13}C$ (‰ PDB-1)	$\delta^{18}O$ (‰ PDB-1)	TOC (%)
MT93	226.5	16	Gypsarenite	F6	0.708914	0.708916	23.1			0.03
MT90	220.3	16	Gypsrudite	F6						0.03
MT94	218.8	16	Gypsrudite	F6	0.708900		22.7			
MT96	218.3	16	Bituminous shale	F1						0.16
MT95	218	16	Selenite	F5	0.708890		22.6			0.01
MT89	217.8	15	Selenite	F5	0.708900		23.3	−0.45	−0.82	0.04
MT88	216	15	Nodular and lenticular selenite	F5	0.708914	0.708930	23.2	−2.32	−2.91	0.04
MT87	210.6	15	Banded selenite	F4	0.708923	0.708940	23.2	−0.06	−1.75	0.03
MT85	207.2	15	Selenite with limestone	F6				−5.48	−5.88	0.02
MT83	206.8	15	Selenite	F5				−5.32	−4.86	0.02
MT82	206	15	Selenite	F5				−5.81	−5.20	0.03
MT81	203.7	15	Massive selenite	F3	0.708899		23.6			0.03
MT80b	203.3	15	Massive selenite with limestone	F3				−3.23	5.12	0.18
MT80	203.3	15	Massive selenite	F3						0.41
MT79	202.5	14	Bituminous shale	F1						0.88
MT77	200.5	14	Nodular and lenticular selenite	F5	0.708954	0.708943	22.5			
MT76	188.5	14	Banded selenite with limestone	F4	0.708950	0.709001	22.2	−3.11	−5.02	0.04
MT75	187	14	Massive selenite with limestone	F3	0.708893		23.3	−1.96	−3.61	
MT74	185.5	13	Nodular and lenticular selenite	F5	0.709024	0.708910				0.06
MT73	185	13	Banded selenite	F4	0.708910	0.708900				0.14
MT72	184.5	13	Massive selenite	F3						0.24
MT70	184	13	Massive selenite	F3	0.708920		22.9			
MT100	180.5	12	Selenite	F6	0.708948	0.708974	22.4			
MT99	176.5	12	Nodular and lenticular selenite	F5	0.708921	0.708944	22.2			0.12
MT98	172.8	12	Banded selenite	F4	0.708923	0.708923	22.8			
MT97	169.3	12	Massive selenite	F3	0.708943		22.6			0.03
MT67	167	11	Nodular and lenticular selenite	F5	0.708893		23.0	−0.45	−2.67	0.02
MT66	165.7	11	Nodular and lenticular selenite	F5	0.708951	0.708933	21.8			0.03
MT65	161	11	Banded selenite	F4	0.708900	0.708930	22.9			
MT64	158	11	Massive selenite	F3	0.708920		22.3			
MT62	157	10	Bituminous shale	F1						0.73
MT61b	155	10	Nodular and lenticular selenite	F5	0.708900		22.9			
MT61a	155	10	Nodular and lenticular selenite	F5	0.708971	0.708940	23.1			
MT60	150.5	10	Banded selenite	F4	0.709000	0.708960	23.2			
MT59	149	10	Massive selenite	F3	0.708895		22.8			
MT58	148.8	9	Bituminous shale	F1						0.48
MT57	148.5	9	Selenite	F6	0.708923		22.8			

MT56	147.5	9	Banded selenite with limestone	F4				−1.63	−4.05	0.06
MT55	143.5	9	Banded selenite with limestone	F4						0.24
MT54	143	9	Bituminous shale	F1						1.3
MT53b	141.5	9	Nodular and lenticular selenite	F5	0.708945		23.7			
MT53a	141.5	9	Nodular and lenticular selenite	F5	0.709000	0.709010	22.9	−2.5	−1.68	
MT53	141.5	9	Banded selenite	F4			23.4			
MT52	139	9	Banded selenite with limestone	F4	0.709018	0.708979	22.9			0.05
MT51	137	9	Massive selenite	F3	0.708934		23.0			0.04
MT50	136.5	8	Bituminous shale	F1						0.96
MT49	136	8	Selenite	F5						0.07
MT48b	135.5	8	Nodular and lenticular selenite	F5	0.708920		23.6			
MT48a	135.5	8	Nodular and lenticular selenite	F5	0.708940	0.708940	22.7			
MT48	135.5	8	Nodular and lenticular selenite	F5			23.7			
MT47	134	8	Banded selenite with limestone	F4	0.708965	0.709014	23.3	−0.8	−4.39	0.06
MT46	130.5	8	Massive selenite	F3	0.708931		23.4			0.04
MT39	130.3	7	Bituminous shale	F1						1.38
MT37	129	7	Nodular and lenticular selenite	F5						0.04
MT36	126.5	7	Banded selenite with limestone	F4				−1.04	5.76	0.06
MT35	120.5	7	Massive selenite	F3						
MT34	119.7	7	Stromatolite	F2				1.77	−3.64	0.11
MT31	118.0	6	Banded selenite	F4						0.07
MT29	107.8	6	Nodular and lenticular selenite	F5	0.708900		23.3			
MT27b	104.3	6	Nodular and lenticular selenite	F5	0.709020		23.1			
MT27a	104.3	6	Banded selenite	F4	0.708900		22.5			
MT26	102	6	Banded selenite	F4	0.708920		23.3			
MT25	99	6	Massive selenite with limestone	F3				−3.11	3.34	0.05
MT24	95.5	6	Massive selenite	F3	0.708910		22.6			
MT23	94.5	6	Bituminous shale	F1						0.97
MT21	93.5	6	Massive selenite	F3	0.708910		22.7			0.08
MT20	92.5	6	Stromatolite (carbonate)	F2		0.708920		−0.83	4.95	0.14
MT19	92.3	5	Selenite	F6	0.708910		22.6			
MT18	91	5	Massive selenite	F3	0.708910		22.8			
MT17	75.2	5	Banded selenite with limestone	F4	0.708920		22.6	−4.74	6.05	0.1
MT16	69	5	Massive selenite	F3	0.708900		22.4			0.05
MT11	37.8	4	Massive selenite	F3	0.708930		23.0	−6.16	0.07	0.03
MT10	37.3	4	Stromatolite	F2		0.708930		−14.68	−2.85	0.07
MT12	36.5	3	Limestone	F5				−5.77	−6.40	0.03
MT13	36.3	3	Selenite-bearing limestone	F5	0.708900		23.4	−6.67	−4.62	
MT14	36	3	Massive selenite	F3	0.708940		23.2			0.03
MT09	18.2	3	Bituminous shale pocket	F3						3.13
MT05	11.3	3	Massive selenite	F3	0.708930		22.9			
MT04	10	3	Stromatolite (carbonate)	F2		0.708900		1.25	5.02	
MT02	5.5	2	Massive selenite	F3	0.708930		23.6			0.04
MT01	0	1	Massive selenite	F3	0.708920		23.2			

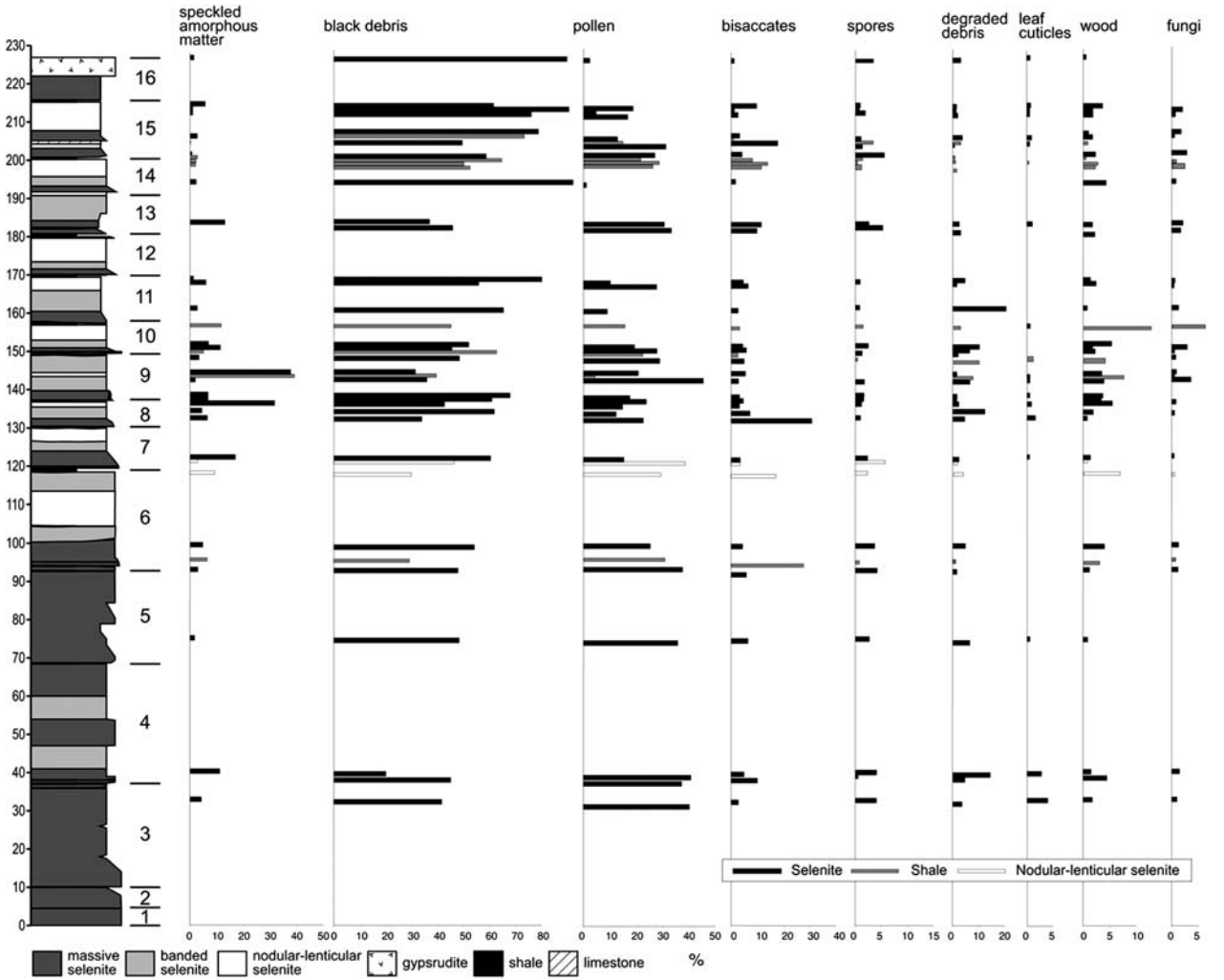

Fig. 2. Organic matter characterization of the Vena del Gesso section.

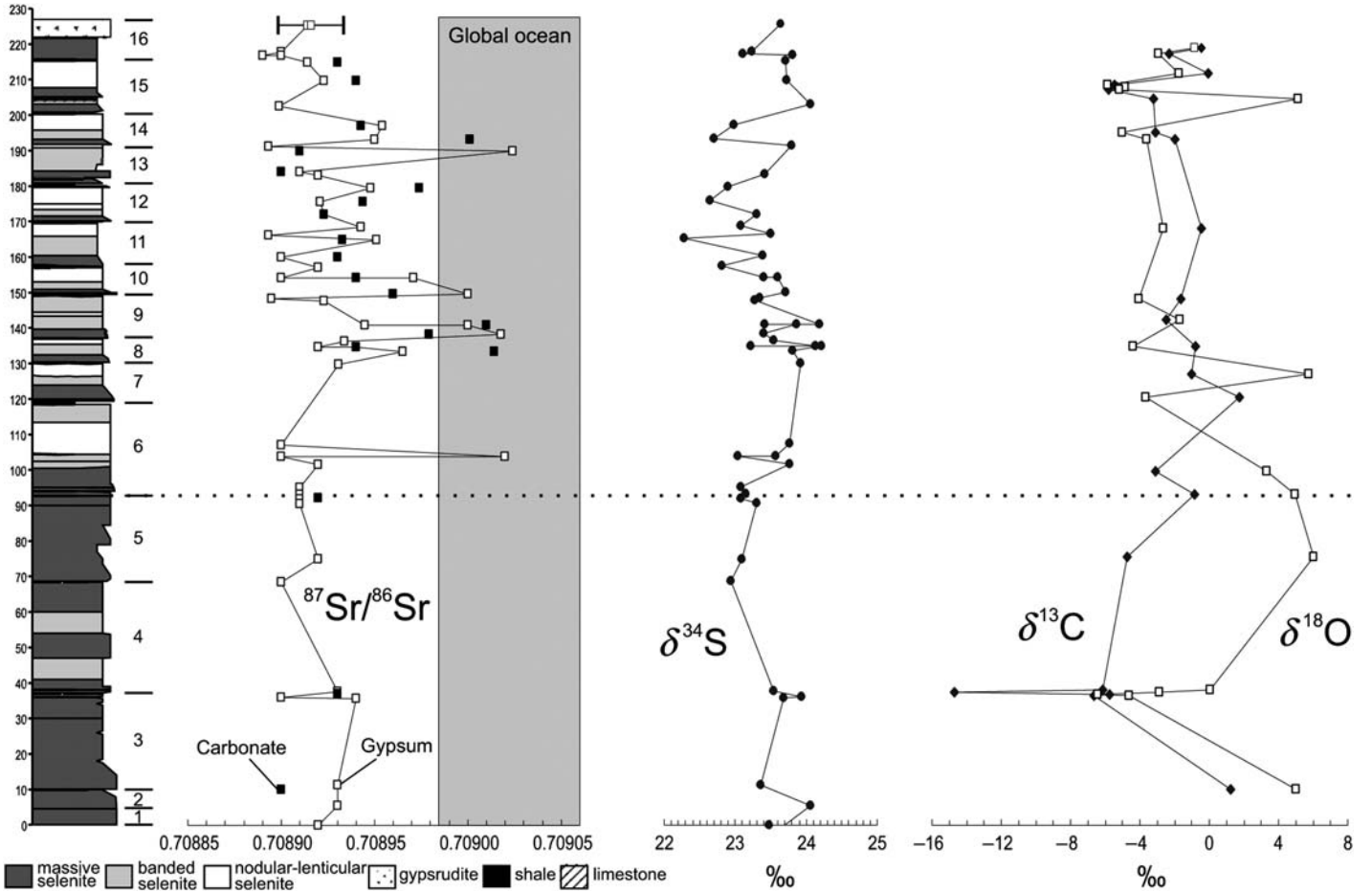

Fig. 3. Isotope geochemistry of the Vena del Gesso section. Global ocean values from McArthur *et al.* (2001).

carbon data indicate continental water inputs and a possible significant contribution of isotopically light carbon from organic matter reduction. The lowest carbon value ($\delta^{13}C = -14.68$ sample MT 10) is from a laminar stromatolite layer rich in algal filaments (Table 2). These data suggest a complex origin of the carbonates by mixing of marine and non-marine waters with a significant contribution of organic matter reduction, as suggested for the Messinian of the Nijar basin, Spain (Lu *et al.* 2001).

Discussion

The geochemical data and the organic matter association seem to point to an evaporite basin dominated by continental waters which received significant marine recharges. Seawater inputs have been detected only in the upper part and are concomitant with a marked facies change starting from the 6° bed where nodular, lenticular and flaser bedded gypsum (F5 of Vai & Ricci Lucchi 1977) appear for the first time upsection.

Variations of stable isotopes thorough section suggest that the strongest evaporating conditions during carbonate formation were common in the lower part. A significant contribution of continental water marks the passage from the 3° to the 4° beds. The upper part of the section is dominated by freshwater inputs and only two phases of strong evaporitic conditions are revealed by high $\delta^{18}O$ values in the carbonates from the 7° and 15° beds (Fig. 3).

It is interesting to note that the highest $\delta^{18}O$ values of carbonates that indicate strongly evaporating conditions are not found at the same stratigraphic levels where the associated sulphates show their higher $\delta^{34}S$ values. In particular, the highest $\delta^{18}O$ values do not match the highest Sr isotope ratios of carbonate samples and are also widely distributed in the lower part of the section, where Sr isotopes indicate a prevailing proportion of freshwater over seawater. This apparent contradiction is probably due to the fact that $^{87}Sr/^{86}Sr$ is insensitive to salinity change and evaporation conditions, but is directly controlled by simple mixing of ocean and river water (Flecker *et al.* 2002). On the other hand, $\delta^{34}S$ and stable isotopes in carbonates are less sensitive, with respect to Sr isotopes, in detecting marine to non-marine influence during evaporite deposition. Moreover, Sr isotopes are more sensitive to restriction of ocean exchange than fauna and lithology when net-evaporation is positive (Flecker & Ellam 2006). The highest recorded $\delta^{34}S$ values may be related to some degree of gypsum recycling from the basin margins and the similar trend of the $\delta^{34}S$ and Sr ratio curves may indicate that these conditions were possibly concomitant with the marine ingressions.

In a marginal basin such as the Vena del Gesso, which records the northernmost environmental conditions during the salinity crisis, the influences of continental waters may have been stronger than in any other Mediterranean setting. These conditions are recorded by the palinology of the shales intercalations which, in contrast with Sicily, suggests a forested environment, the absence of severe dry conditions and the presence of swampy areas (Bertini 2002). On the other hand, significant departures from Sr oceanic values are documented by scattered data in the Lower Evaporites of the Mediterranean (Flecker *et al.* 2002) and we have observed a similar dramatic facies change in the gypsum sections of Spain, Crete, Tuscany, Calabria and Sicily. If these considerations are correct, then we have new markers that support an attempt of a large scale correlation for the Lower Evaporites. Rates of inflow condition variations (Atlantic exchange) may have triggered the gypsum facies associations across the entire Mediterranean.

Conclusions

This is the first detailed isotope geochemistry and organic matter characterization of a Lower Evaporite section that is well constrained from the stratigraphic point of view. The results indicate that the Vena del Gesso marginal basin was dominated by continental water-derived brines and received repeated pulses of oceanic water in the upper part. The onset of oceanic water recharge coincides with a marked change in facies association producing the nodular, lenticular and flaser bedded gypsum (F5 of Vai & Ricci Lucchi 1977), which appear for the first time starting from the 6° bed.

Because seawater recharges and a similar facies change are present also in other Messinian sections, the implication of these results is that we have new possible geochemical and facies markers to correlate the Lower Evaporite sediments across the Mediterranean. These oceanic signals revealed by geochemistry and facies change also may have been preserved in the succession of the deep Mediterranean, which has not been investigated in detail.

We thank BPB Italia for permission to sample the Monte Tondo quarry. The manuscript has benefited from the constructive review of R. Flecker, C. Pierre and B. C. Schreiber.

References

AHARON, P., GOLDSTEIN, S. L., WHEELER, C. W. & JACOBSON, G. 1993. Sea-level events in South Pacific linked with the Messinian Salinity Crisis. *Geology*, **21**, 771–775.

BARCHI, M., DE FEYTER, A., MAGNANI, M. B., MINELLI, G., PIALLI, G. & SOTERA, B. M. 1998. The structural style of the Umbria-Marche fold and thrust belt. *Memorie della Società Geologica Italiana*, **52**, 557–578.

BASSETTI, M. A., MANZI, V., LUGLI, S, ROVERI, M. A., LONGINELLI, RICCI LUCCHI, F. & BARBIERI, M. 2004. Paleoenvironmental significance of Messinian post-evaporitic lacustrine carbonates in the northern Apennines, Italy. *Sedimentary Geology*, **172**, 1–18.

BERTINI, A. 2002. Palynological evidence of upper Neogene environments in Italy. *Acta Universitatis Carolinae–Geologica*, **46**(4), 15–25.

CENDÓN, D. I., PERYT, T. M., AYORA, C., PUEYO, J. J. & TABERNER, C. 2004. The importance of recycling processes in the Middle Miocene Badenian evaporite basin (Carpathian foredeep): Paleoenvironmental implications. *Palaeogeography, Palaeoclimatology, Palaeoecology*, **212**, 141–158.

DINELLI, E., TESTA, G., CORTECCI, G. & BARBIERI, M. 1999. Stratigraphic and petrographic constraints to trace element and isotope geochemistry of Messinian sulfates of Tuscany. *Memorie della Società Geologica Italiana*, **54**, 61–74.

FLECKER, R. & ELLAM, R. M. 1999. Distinguishing climatic and tectonic signal in the sedimentary successions of marginal basins using Sr isotopes: an example from the Messinian salinity crisis, Eastern Mediterranean. *Journal of the Geological Society of London*, **156**, 847–854.

FLECKER, R. & ELLAM, R. M. 2006. Identifying Late Miocene episodes of connection and isolation in the Mediterranean–Paratethyan realm using Sr isotopes. *Sedimentary Geology*, **188–189**, 189–203.

FLECKER, R., DE VILLIERS, S. & ELLAM, R. M. 2002. Modelling the effect of evaporation on the salinity–$^{87}Sr/^{86}Sr$ relationship in modern and ancient marginal–marine systems: the Mediterranean Messinian Salinity Crisis. *Earth Planetary Science Letters*, **203**, 221–233.

HOLSER, W. T. 1977. Catastrophic chemical events in the history of the ocean. *Nature*, **267**, 403–408.

KEOGH, S. M. & BUTLER, R. W. H. 1999. The Mediterranean water body in the late Messinian: interpreting the record from marginal basins on Sicily. *Journal of the Geological Society of London*, **156**, 837–846.

KLINKHAMMER, G. P. & LAMBERT, C. E. 1989. Preservation of organic matter during salinity excursions. *Nature*, **339**, 271–274.

KRIJSMANN, W., HILGEN, F. J., MARABINI, S. & VAI, G. B. 1999. New paleomagnetic and cyclostratigraphic age constraints on the Messinian of the Northern Apennines (Vena del Gesso Basin, Italy). *Memorie della Società Geologica Italiana*, **54**, 25–33.

LONGINELLI, A. 1979. Isotope geochemistry of some Messinian evaporites; paleoenvironmental implications. *In*: CITA, M. B. & WRIGHT, R. (eds) *Geodynamic and Biodynamic Effects of the Messinian Salinity Crisis in the Mediterranean*. Paleogeography, Paleoclimatology, Paleoecology, **29**, 95–123.

LU, F. H. & MEYERS, W. 2003. Sr, S, and SO_4 isotopes and depositional environments of the upper Miocene evaporites, Spain. *Journal of Sedimentary Research*, **73**, 444–450.

LU, F. H., MEYERS, W. J. & SCHOONEN, M. A. A. 2001. $\delta^{34}S$ and $\delta^{18}O$ (SO_4) fractionation modeling and environmental significance. *Geochimica et Cosmochimica Acta*, **65**, 3081–3092.

LUGLI, S., MANZI, V., ROVERI, M. & SCHREIBER, B. C. 2005. The Messinian Lower Evaporites in the Mediterranean: a new facies model. FIST Forum Geoitalia 2005, 22–23 September 2005, Spoleto (italy), Abstract book, 2.

MCARTHUR, J. M., HOWARTH, R. J. & BAILEY, T. R. 2001. Strontium isotope stratigraphy: LOWESS version 3: Best fit to the marine Sr-isotope curve for 0–509 Ma and accompanying look-up table for deriving numerical age. *Journal of Geology*, **109**, 155–170.

MANZI, V., LUGLI, S., RICCI LUCCHI, F. & ROVERI, M. 2005. Deep-water clastic evaporites deposition in the Messinian Adriatic foredeep (northern Apennines, Italy): did the Mediterranean ever dry out? *Sedimentology*, **52**, 875–902.

MARABINI, S. & VAI, G. B. 1985. Analisi di facies e macrotettonica della Vena del Gesso in Romagna. *Bollettino della Società Geologica Italiana*, **104**, 21–42.

MATANO, F., BARBIERI, M., DI NOCERA, S. & TORRE, M. 2003. Stratigraphy and strontium geochemistry of Messinian evaporite-bearing successions of the southern Apennines foredeep, Italy: implications for the Mediterranean 'salinity crisis' and regional palaeogeography. *Palaeogeography, Palaeoclimatology, Palaeoecology*, **217**, 87–114.

MÜLLER, D. W. & MUELLER, P. A. 1991. Origin and age of the Mediterranean Messinian evaporites: implications from Sr isotopes. *Earth Planetary Science Letters*, **107**, 1–12.

PIERRE, C. 1982. *Teneurs en isotopes stables (^{18}O, ^{2}H, ^{13}C, ^{34}S) et conditions de genèse des évaporites marines: application à quelques milieux actuels et au Messinien de Méditerranée*. Unpublished doctoral thesis. Université Paris-Sud Orsay.

PIERRE, C. & FONTES, J. C. 1978. Isotope composition of Messinian sediments from the Mediterranean Sea as indicators of paleoenvironments and diagenesis. *Initial Reports of the Deep Sea Drilling Project*, **42**, 635–650.

PIERRE, C. & ROUCHY, J. M. 1990. Sedimentary and diagenetic evolution of Messinian evaporites in the Tyrrhenian Sea (ODP Leg 107, Sites 652, 653 and 654): petrographic, mineralogical, and stable isotope records. *In*: KASTENS, K. A. & MASCLE, J. (eds) *Proceedings of the Ocean Drilling program, Scientific Results*, **107**, 187–201.

RAAB, M. & SPIRO, B. 1991. Sulfur isotopic variations during seawater evaporation with fractional crystallization. *Chemical Geology*, **86**, 323–333.

REES, C. E. 1978. Sulphur isotope measurements using SO_2 and SF_6. *Geochimica et Cosmochimica Acta*, **42**, 383–389.

REES, C. E., JENKINS, W. J. & MONSTER, J. 1978. The sulfur isotopic composition of ocean water sulfate. *Geochimica et Cosmochimica Acta*, **42**, 377–381.

RICCI LUCCHI, F. 1986. The foreland basin system of the Northern Apennines and related clastic wedges: a preliminary outline. *Giornale di Geologia*, **48**(1–2), 165–186.

RICCHIUTO, T. & MCKENZIE, J. 1978. Stable isotope investigation of Messinian sulfate samples from DSDP Leg 42A, Eastern Mediterranean Sea. *In*: HSÜ, K. J. *ET AL.* (eds) *Initial Reports of Deep Sea Drilling Project*, **42**, 657–660.

ROUCHY, J.-M. & PIERRE, C. 1990. Sedimentary and diagenetic evolution of Messinian evaporites in the Thyrrenian Sea (ODP Leg 107, sites 652, 653, and 654); petrographic, mineralogical, and stable isotope records. *Proceedings of the Ocean Drilling Program, Thyrrenian Sea*, **107**, 187–210.

ROVERI, M., BASSETTI, M. A. & RICCI LUCCHI, F. 2001. The Mediterranean Messinian Salinity Crisis: an Apennine foredeep perspective. *Sedimentary Geology*, **140**, 201–214.

ROVERI, M., LANDUZZI, A., BASSETTI, M. A., LUGLI, S., MANZI, V., RICCI LUCCHI, F. & VAI, G. B. 2004. The record of Messinian events in the Northern Apennines foredeep basins. B19 Field trip guidebook. 32nd International Geological Congress, 20–28 August 2004.

ROVERI, M., MANZI, V., BASSETTI, M. A., MERINI, M. & RICCI LUCCHI, F. 1998. Stratigraphy of the Messinian post-evaporitic stage in eastern-Romagna (northern Apennines, Italy). *Giornale di Geologia*, **60**, 119–142.

ROVERI, M., MANZI, V., RICCI LUCCHI, F. & ROGLEDI, S. 2003. Sedimentary and tectonic evolution of the Vena del Gesso basin (Northern Apennine, Italy): Implications for the onset of the Messinian salinity crisis. *Geological Society of America Bulletin*, **115**, 387–405.

THODE, H. G. & MONSTER, J. 1965. Sulfur isotope geochemistry of petroleum, evaporites and ancient seas. *American Association of Petroleum Geologists, Memoir* **4**, 367–377.

VAI, G. B. 1988. A field trip guide to the Romagna Apennine geology – the Lamone Valley. *In*: DE GIULI, C. & VAI, G. B. (eds) *Fossil Vertebrates in the Lamone Valley, Romagna apennines*. Field Trip Guidebook, International Workshop: Continental Faunas at the Mio-Pliocene Boundary, Faenza, 28–31 March 1988, Litografica Faenza, Faenza, Italy, 7–37.

VAI, G. B. 1997. Cyclostratigraphy estimate of the Messinian stage duration. *In*: MONTANARI, A., ODIN, G. S. & COCCIONI, R. (eds) *Miocene Stratigraphy: an integrated approach*. Elsevier Science, Amsterdam, 463–476.

VAI, G. B. & RICCI LUCCHI, F. 1977. Algal crusts, autochtonous and clastic gypsum in a cannibalistic evaporite basin; a case history from the Messinian of Northern Apennine. *Sedimentology*, **24**, 211–244.